ACS Catalysis

RESEARCH ARTICLE

pubs.acs.org/acscatalysis

Interplay between Anomalous Transport and Catalytic Reaction Kinetics in Single-File Nanoporous Systems

Da-Jiang Liu,[†] Jing Wang,[†,‡] David M. Ackerman,[†,§] Igor I. Slowing,[†] Marek Pruski,[†,§] Hung-Ting Chen,[†] Victor S.-Y. Lin,[†,§] and James W. Evans*[,†,‡,∥]

[†]Ames Laboratory—USDOE, and [‡]Departments of Mathematics, [§]Chemistry, and [∥]Physics & Astronomy, Iowa State University, Ames Iowa 50011, United States

ABSTRACT: Functionalized nanoporous materials have broad utility for catalysis applications. However, the kinetics of catalytic reaction processes in these systems can be strongly impacted by the anomalous transport. The most extreme case corresponds to single-file diffusion for narrow pores in which species cannot pass each other. For conversion reactions with a single-file constraint, traditional mean-field-type reaction-diffusion equations fail to capture the initial evolution of concentration profiles, and they cannot describe the scaling behavior of steady-state reactivity. Hydrodynamic reaction-diffusion equations accounting for the single-file aspects of chemical diffusion can describe such initial evolution, but additional refinements are needed to incorporate fluctuation effects controlling, for example, steady-state reactivity localized near pore openings. For polymerization reactions with a single-file constraint, initial behavior depends strongly on system details such as catalytic site loading and reaction rate. However, long-time behavior often involves the formation of a dominant large polymer near each end of the pore, initially within the pore but subsequently partly extruding. In this partial extrusion regime, the kinetics is governed by the special features of the random walk describing the motion of the end of the partly extruded polymer, noting that this extruded end must return within the pore for further growth.

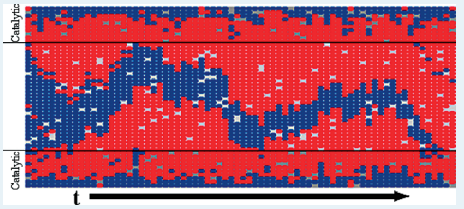

KEYWORDS: single-file diffusion, catalytic reaction, nanoporous materials, lattice-gas models, KMC

1. INTRODUCTION

Advances in the synthesis of functionalized porous materials, either microporous zeolites (aluminosilicates) or mesoporous silica nanoparticles (MSNs), have provided significant opportunities for the development of new catalytic systems.[1−4] Pore diameters for zeolites are in the range of 1−2 nm[1] and those for MSNs range from 2 to 10 nm.[2] We note that the effective diameter for pores in MSNs can be even smaller than the nominal ∼2 nm minimum after functionalization with catalytic sites. Our focus is on the regime of small pore diameters no larger than ∼2 nm. Clearly, small pore diameters provide a mechanism for selectivity. However, it is also the case that diffusive transport within such pores can be severely restricted. In the extreme case, transport within one-dimensional (1D) linear pores corresponds to so-called single-file diffusion where molecules cannot pass each other. Naturally, there have been extensive studies of transport in single-file systems, often emphasizing the anomalous nature of tracer- or self-diffusion.[5,6] This anomaly is reflected in a sublinear increase with time in the mean-square displacement of a specific "tagged" particle.[7,8] Such behavior contrasts the linear increase for conventional diffusion. However, of additional interest for catalysis, and the focus of this contribution, is the *interplay* between this type of anomalous transport and the catalytic reaction kinetics.

The above examples constitute a special class from among general reaction-diffusion processes, which are traditionally described by mean-field reaction-diffusion equations (RDE).[9,10] These RDE include a conventional mean-field treatment of chemical kinetics which ignores spatial correlations in the reactant distribution. Such RDE typically also include a simplified treatment of chemical diffusion with constant Fickian diffusion coefficients and independent transport of different species. Note that chemical or collective diffusion describes the diffusion flux induced by concentration gradients[11] and is distinct from the tracer diffusion mentioned above. We remark that heterogeneous catalytic reactions on two-dimensional (2D) surfaces have been effectively treated by mean-field RDE.[12] However, it is well recognized that interactions between chemisorbed reactants can produce islanding or ordering, and thus non-mean-field kinetics.[13] The complexities of diffusion in mixed reactant adlayers are less appreciated.[14] Nonetheless, such complications can be appropriately treated by realistic atomistic-level modeling.[15,16]

In contrast, for 1D nanoporous reaction-diffusion systems, there is a broad appreciation of complexities of diffusion as well as analysis of certain aspects of chemical (as well as tracer) diffusion.[6,17,18] There has also been some development of approximate RDE for simple catalytic reaction models.[19−21] One might anticipate that the restricted nature of transport in these systems (as well as interactions between reactants) could induce spatial correlations in the reactant distributions, and thus deviations from mean-field reaction kinetics. The nature of the reaction kinetics, and also the interplay with chemical diffusion, have been

Special Issue: Victor S. Y. Lin Memorial Issue

Received: February 26, 2011
Revised: May 13, 2011
Published: May 17, 2011

explored in some simulation studies.[19−25] However, such analyses are limited and the current understanding is far from complete. Thus, the goal of this study is to provide a perspective on recent developments and also to contribute new results in the analysis of catalytic conversion and polymerization reactions in nanoporous single-file systems.

Conversion reactions (A→B) in 1D nanoporous systems with single-file diffusion have been the subject of the most extensive analyses.[19−26] It should be emphasized that for systems with inhibited passing or a strict single-file constraint, the key factor impacting reactivity is the extent to which reactants and products A and B can pass each other. The influence on reactivity of the extent of passing of reactants A with each other, and products B with each other, is relatively minor. One general expectation emerging already from earlier studies of a generic A→B conversion model with single-file diffusion[24] is that reactivity is localized near the pore openings. Various single-file conversion reactions have been considered in zeolites, including a detailed study of Pd-catalyzed neopentane conversion.[25] Our motivation here comes from studies of various conversion reactions, such as Beckman rearrangement,[27,28] in functionalized MSNs with narrow pores. In some cases, the effective diameter of the pores is reduced below 2 nm by functionalization with the catalytic group. Then, larger reactant and product species cannot pass, at least not without difficulty because of the need for orientational alignment with each other and with the pore axis. We are also interested in more general catalytic transformations involving two reactants ($A + A' \rightarrow B$) subject to inhibited passing or a strict single-file constraint for A and B. These processes can be analyzed using the simpler A→B conversion models provided that A′ is sufficiently small so that it can readily pass both A and B, and provided that A′ is present in excess. Examples of this type might be the nucleophilic catalytic reactions in MSNs functionalized with the bulky dialkylaminopyridine (DMAP-MSN),[29] and the Diels−Alder reaction in urea or thiourea-functionalized MSNs.[30] As discussed further below, of particular interest for our modeling of the effects of anomalous transport is a study of the conversion of *p*-nitrobenzaldehyde (PNB) to an aldol compound in amine-functionalized MSNs where the dependence of reactivity on effective pore diameter has been quantified.[31]

Fundamental questions for these conversion reactions still requiring resolution include the following:

(i) How does overall reactivity depend on basic parameters such as the intrinsic rate of reaction for reactant species in the vicinity of a catalytic site and on species' mobility within the pore?
(ii) How does the propensity for passing of various reactant and product species within the pore (which depends strongly on pore diameter) affect the overall reactivity?
(iii) How does the distribution of catalytic sites affect overall reactivity, particularly catalytic functionalization restricted to near the pore openings versus uniformly throughout the entire pore?
(iv) To what extent can the evolution of concentration profiles and thus reactivity be described within a traditional deterministic mean-field-type RDE picture as opposed to being controlled by stochastic effects (e.g., fluctuations in numbers of adsorbing and desorbing species at the pore openings)?
(v) Can shortcomings of traditional RDE approaches be overcome by refined treatments?

In this study, we consider simple A→B and sequential A→B→C conversion reaction mechanisms, and provide new insights and modeling strategies addressing the above issues.

Polymerization reactions have received very little attention, particularly with regard to modeling for single-file systems.[32,33] However, strong motivation for such studies derives from the use of mesoporous materials to facilitate production and processing of polymeric materials with desired higher-order structures, for example, linear "molecular wires" versus more complex cross-linked networks.[4] Another motivation derives from interest in the formation of composite nanomaterials, for example, by encapsulating conducting polymers within mesoporous materials. There have been several studies demonstrating the potential for using MSNs to achieve these ends.[34−37] Of particular focus for our model development was a previous study which considered oxidative catalyzed formation of poly(phenylene butadinylene) polymer (PPB) in Cu^{2+}-functionalized MCM-41 silica.[34] For this PPB mechanism ($A + A_n \rightarrow A_{n+1}$), previous modeling in the regime of diffusion-limited reaction regime for low catalyst loading indicated predominant polymer growth near pore openings, and also anomalous non-Markovian growth kinetics.[32,33] Additional modeling is needed for the experimentally relevant reaction-limited regime with high catalyst loading.

Fundamental open questions for these types of polymerization reactions include the following:

(i) What are the basic spatiotemporal features of polymer growth, that is, the location and distribution of dominant growing polymers, and characteristics of the polymer growth kinetics?
(ii) How does the above spatiotemporal picture depend on basic parameters such as intrinsic reactivity, the variation of oligomer mobility with length, the distribution of catalytic sites, and so forth?
(iii) For more complex cross-coupling polymerization mechanisms, for example, A + B→AB, B + AB..→BAB.., and so forth, does the pore quickly fill with small oligomers which cannot react because of neighboring ends of the same type, or can significant polymer growth be achieved?
(iv) Can traditional Markovian rate equations describe polymer growth kinetics and length distributions, or are alternative formulations required?

In this study, we provide further analysis for the PPB polymerization reaction mechanism ($A + A_n \rightarrow A_{n+1}$) described above. In addition, we also develop a model for the Sonagashira cross-coupling polymerization reaction mechanism (A + B→AB, etc.) motivated by experiments for formation of poly(*p*-phenylene ethynylene) (PPE) polymers using Pd(II)-functionalized MSNs.[38] In both cases, we focus on the case of high catalyst loading and the regime of reaction-limited polymerization which is relevant to experimental studies. A universal spatiotemporal picture is obtained for both mechanisms, and we develop and apply concepts from continuous-time random walk (CTRW) theory to address the shortcomings of traditional chemical kinetics.

To treat the spatial aspects of these single-file reaction-diffusion processes, previous modeling had often incorporated the feature that both reactants and products inside the pore reside at the sites of a discrete grid or linear lattice.[19−26,32,33] Single-file diffusion is readily incorporated by a no-passing constraint in the particle hopping dynamics (where multiple occupancy

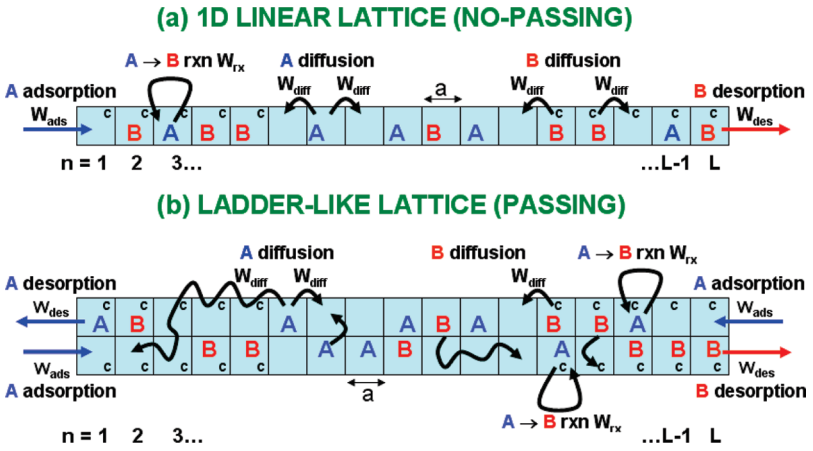

Figure 1. Schematic of the A→B conversion reaction (rxn) model with hopping only to nearest-neighbor (NN) empty sites within a pore described by (a) a 1D linear lattice (no passing); (b) a ladder-like lattice (passing). Here, only sites near pore ends are catalytic "c", and desorption and hopping rates for A and B are equal; n labels sites in the direction along the pore axis.

of a single site is also excluded). Adopting a discrete spatial structure should not affect the basic aspects of model behavior, at least for smoothly varying concentration profiles over several lattice constants. Such lattice-gas (LG) modeling also greatly facilitates both analytic investigation and Kinetic Monte Carlo (KMC) simulation of the model, and thus is adopted here.

In Sec.2, we describe the conversion reaction models analyzed in this study, together with the hierarchical form of the associated exact master equations. In Sec.3, we present hydrodynamic RDE formulations for continuous coarse-grained versions of the models. Precise results from KMC simulations are compared with predictions from various analytic formulations in Sec.4. In Sec.5, we describe our models for catalytic polymerization for both the PPB $A + A_n \rightarrow A_{n+1}$ and Sonagashira-type mechanisms. In Sec.6, we characterize behavior in various reaction-rate regimes and present associated results from KMC simulations. Exploiting concepts from random walk theory, we provide further insight into behavior in the partial-extrusion regime in Sec.7. Conclusions are provided in Sec.8.

2. CONVERSION REACTIONS: MODELS AND MASTER EQUATIONS

2A. Models. First, we describe a general class of models for the diffusion-mediated catalytic conversion of a reactant to a product (A → B) inside narrow pores. Reactants and products are localized to sites of a 1D linear lattice traversing the pore, or more generally to sites on a ladder (see Figure 1). The separation between adjacent sites is given by the lattice constant "a" which is selected to be comparable to the reactant and product size (~1 nm). The simplest scenario for diffusion is that A and B hop to adjacent empty sites. This prescription corresponds to single-file diffusion with a strict no-passing constraint on the 1D linear lattice, but not on the ladder. One could allow positional exchange of adjacent A and B on the 1D linear lattice to relax the strict single-file constraint, noting that exchange of adjacent particles of the same type has no effect. (Allowing longer hops over other particles would also relax the constraint.) On the other hand, one could impose a nearest-neighbor (NN) exclusion constraint on the linear ladder which would enforce no-passing. One has considerable flexibility treating diffusive dynamics! The other mechanistic steps in the model are adsorption of external reactant species A at terminal sites of the pore provided that these sites are unoccupied or empty (E); conversion A → B at catalytic sites (c) within the pore; and desorption of both the reactant, A, and product, B, from terminal sites of the pore. The catalytic sites may constitute all sites or various subsets of sites within the pore. These mechanistic steps and a configuration with catalytic sites just near the pore openings are also illustrated in Figure 1. The total reactivity (i.e., the total production rate of B) is proportional to the total amount of A within the catalytic regions of the pore. Sequential conversion reactions, for example, A → B → C, could also be considered.

2B. Hierarchical Master Equations. We first formulate our model for a general sequential conversion reactions A → B → C→... (including A→B as a special case) on a linear lattice. Sites in the pore are labeled by $n = 1, 2,..., L$ (for pore length L), so that the terminal sites are $n = 1$ and $n = L$. Allowing only hopping to NN empty sites results in strict single-file diffusion, but this constraint is relaxed if one includes exchange of NN particles. Rates for the various processes will be denoted by $W_{ads}(A) = W_{ads}$ for adsorption of A; $W_{des}(K)$ for desorption of species K = A, B,..; $W_{diff}(K)$ for hopping to NN empty sites for K; $W_{ex}(K|K')$ for exchange of NN K and K′; and $W_{rx}(A)$ for A → B conversion, and so forth. An exact analytical description of such stochastic Markov processes is provided by the *master equations* for the evolution of probabilities of various configurations for the entire system.[39] Often these are written in *hierarchical form*.[19−23] Here, we use $\langle K_n \rangle$ to denote the probability or ensemble averaged concentration for species K at site n, $\langle K_n E_{n+1} \rangle$ for the probability that K is at site n and for site $n + 1$ to be empty (E), and so forth. Then, the lowest-order equations in the hierarchy describe the evolution of the probabilities for individual sites to be occupied by various species.

For just A→B conversion in the case where *all sites are catalytic*, one has that

$$d\langle A_1 \rangle/dt = W_{ads}\langle E_1 \rangle - W_{des}(A)\langle A_1 \rangle - W_{rx}(A)\langle A_1 \rangle - J_A^{1>2} \quad (1a)$$

$$d\langle B_1 \rangle/dt = -W_{des}(B)\langle B_1 \rangle + W_{rx}(A)\langle A_1 \rangle - J_B^{1>2} \quad (1b)$$

$$d\langle A_n \rangle/dt = -W_{rx}(A)\langle A_n \rangle - J_A^{n>n+1} + J_A^{n-1>n}, \quad \text{for} \quad 1 < n < L \quad (1c)$$

dx.doi.org/10.1021/cs200115c |ACS Catal. 2011, 1, 751–763

$$d\langle B_n\rangle/dt = +W_{rx}(A)\langle A_n\rangle - J_B^{n>n+1} + J_B^{n-1>n}, \quad \text{for} \quad 1 < n < L \tag{1d}$$

together with equations for the terminal site $n = L$ similar to those for $n = 1$. In these equations,

$$J_A^{n>n+1} = W_{diff}(A)[\langle A_nE_{n+1}\rangle - \langle E_nA_{n+1}\rangle] + W_{ex}(A|B)[\langle A_nB_{n+1}\rangle - \langle B_nA_{n+1}\rangle] \tag{2}$$

denotes the *net* flux of A from site n to $n + 1$. The expression for $J_B^{n>n+1}$ is similar. The total rate of production of B is given by $R^B_{tot} = W_{rx}(A)\,\Sigma_{n=c}\langle A_n\rangle$, where the sum is over all catalytic sites (i.e., over all sites in this example).

It is instructive to consider the special case where $W_{ex}(A|B) = W_{diff}(A)$, so that transport of A including passing of B is completely unhindered (in some sense the opposite of a strict single-file constraint). Then, it follows that eq 2 reduces exactly to $J_A^{n>n+1} = W_{diff}(A)\,[\langle A_n\rangle - \langle A_{n+1}\rangle]$. An analogous exact reduction of diffusion fluxes was demonstrated by Kutner[40] for a single-species system.

The eqs 1a−1d are coupled to probabilities for various configurations of site pairs. Equations for pair probabilities couple to those for triples, and so forth, thus generating a hierarchy. Pair, triplet, and so forth, probabilities are not simply related to single-site probabilities because of spatial correlations deriving from the reaction-diffusion process. A simple mean-field (MF) factorization approximation, $\langle K_nE_{n+1}\rangle \approx \langle K_n\rangle\langle E_{n+1}\rangle$, and so forth, produces a closed set of discrete reaction-diffusion equations (dRDE) for single-site concentrations, $\langle A_n\rangle$ and $\langle B_n\rangle$, noting that $\langle A_n\rangle + \langle B_n\rangle + \langle E_n\rangle = 1$. A higher-level pair approximation retains pair quantities like $\langle K_nE_{n+1}\rangle$, but factorizes triplet quantities, for example, $\langle K_nM_{n+1}N_{n+2}\rangle \approx \langle K_nM_{n+1}\rangle\langle M_{n+1}N_{n+2}\rangle/\langle M_{n+1}\rangle$, with K, M, N = A, B, or E. This generates a closed set of equations for single-site quantities, $\langle A_n\rangle$ and $\langle B_n\rangle$, and the pair quantities, $\langle K_nM_{n+1}\rangle$, with K, M = A or B.[19−23] Such approximations should not be expected to accurately capture all features of single-file diffusion. It is straightforward to generalize the exact master equations and approximations to the case of more general sequential conversion reactions A→B→C→...

Similar to previous studies of the A → B reaction,[20−23] we will explore this and the more general reaction A→B→C for a parameter choice where the *desorption rates and diffusion rates are equal for all species*, that is, $W_{des}(K) = W_{des}$ and $W_{diff}(K) = W_{diff}$, for K = A, B, and C. There is an important consequence of this rate choice. Suppose one does not discriminate between the identity of particles, but only considers whether sites are empty, E, or filled, X = A + B + ... Then, the particle dynamics corresponds to a pure adsorption−desorption-diffusion process for particles X with *no reaction*. Thus, the single-site concentrations, $\langle X_n\rangle$, satisfy a standard discrete diffusion equation with constant (concentration-independent) diffusion coefficient.[20,22,40,41] Since there is no reaction in the dynamics of particles X, the steady-state corresponds to a conventional Gibbsian grand canonical equilibrium state. Furthermore, since there are no interactions between particles X at different sites, they are randomly distributed in this equilibrium state (i.e., there are no spatial correlations). The equilibrium concentration at each site satisfies $\langle X_n\rangle_{eq} = X_{eq} = W_{ads}/(W_{ads}+W_{des})$.[19−22] Below, we always choose $W_{ads} + W_{des} = 1$ which sets the time-scale.

3. CONVERSION REACTIONS: HYDRODYNAMIC REGIME

In discrete LG reaction-diffusion systems, it is common to consider behavior in the "hydrodynamic regime" where there is sufficient diffusion to produce slowly varying particle concentrations over several lattice constants.[12,14,42] This treatment applies to models where the particles are confined either to a linear lattice or to more general ladder-like lattices.

3A. Hydrodynamic Reaction-Diffusion Equations. In the hydrodynamic regime, behavior is described by continuum hydrodynamic reaction-diffusion equations (hRDE) after coarse-graining. Specifically, for linear or ladder lattices, one sets $x = na$, where n is the lattice site label in the direction along the pore. Then, species concentrations per unit length become functions of a continuous variable $K(x = na) \approx a^{-1}\langle K_n\rangle$ (leaving t-dependence implicit). Thus, $X_m = 1/a$ corresponds to the maximum concentration per unit length. Below, we set $a = 1$.

The hRDE in our A→B conversion reaction model with all sites catalytic for individual species concentrations, $A(x)$ for A, and $B(x)$ for B (leaving implicit the t-dependence), have the form

$$\partial A(x)/\partial t = -W_{rx}(A)A(x) - \partial J_A/\partial x \tag{3a}$$

$$\partial B(x)/\partial t = +W_{rx}(A)A(x) - \partial J_B/\partial x \tag{3b}$$

The total concentration satisfies $X(x) = A(x) + B(x)$, and $E(x) = 1 - X(x)$ gives the concentration of empty sites. If sites within the pore are catalytic only in specific regions (e.g., the peripheral regions), then the reaction terms appear only for those locations. Boundary conditions for eqs 3a−3b at the pore ends reflect the adsorption−desorption dynamics.[22] Description of the diffusion fluxes, J_K, for K = A and B is nontrivial for this mixed lattice-gas, even in the absence of interactions beyond site-exclusion. However, Onsager transport theory[17,18,42] ensures that, for example, the diffusive flux of A has the form

$$J_A = -D_{A,A}\partial A(x)/\partial x - D_{A,B}\partial B(x)/\partial x \tag{4}$$

where the diffusion coefficients $D_{A,K}$ generally depend on species concentrations. A similar expression applies for the flux, J_B, of B. One *simple case* allows exchange of A and B with $W_{ex}(A|B) = W_{diff}(A)$, that is, unhindered transport of A including passing of B, as discussed in Sec.2B. Then, it follows that $D_{A,A} = a^2W_{diff}(A)$ and $D_{A,B} = 0$, that is, the presence of B does not interfere with the diffusion of A.

We will compare predictions of a discrete form of these RDE with results from KMC simulation. The appropriate discretization of the reaction kinetics is clear (e.g., from the exact master equations),[22] and that for the diffusion fluxes is mentioned below. The above formulation naturally extends to sequential conversion reactions, for example, A→B→C.

3B. Diffusion Fluxes for Species-Independent Hop Rates. Here, we consider the case of noninteracting lattice-gases (with exclusion of multiple site occupancy) with two components A and B on linear or ladder lattices and with *equal hop rates* to NN empty sites, so that $W_{diff}(A) = W_{diff}(B) = W_{diff}$, and where exchange can be operative at rate $W_{ex} = W_{ex}(A|B)$. Then, in the hydrodynamic regime, one has that[42−45]

$$\begin{aligned} J_A &= -X(x)^{-1}[D_XA(x) + B(x)D_{tr}(X)]\partial A(x)/\partial x \\ &\quad - X(x)^{-1}A(x)[D_X - D_{tr}(X)]\partial B(x)/\partial x \\ &= -D_X[A(x)X(x)^{-1}]\partial X(x)/\partial x \\ &\quad - D_{tr}(X)X(x)^{-1}[B(x)\partial A(x)/\partial x - A(x)\partial B(x)/\partial x], \end{aligned} \tag{5}$$

dx.doi.org/10.1021/cs200115c |ACS Catal. 2011, 1, 751–763

with $D_X = a^2 W_{diff}$.[46] An analogous expression applies for J_B. $D_{tr} = D_{tr}(X)$ represents the tracer diffusion coefficient for a tagged particle within a dense single-component lattice-gas of concentration $X = X(x)$ with hop rate of W_{diff} to NN empty sites, and where all NN pairs of particles can exchange with rate W_{ex}. For systems with *no single-file constraint*, for example, due to exchange with adjacent particles on a 1D linear lattice, or due to a ladder-like lattice model of pore structure, $D_{tr} = D_{tr}(X)$ is nonzero and depends in a nontrivial way on $X = X(x)$. It should decrease from D_X to 0 as X increases from 0 to 1. In the special case of unhindered exchange with $W_{ex} = W_{diff}$, one has that $D_{tr}(X) = D_X$ for all X. In this case, eq 5 reduces to $J_A = -D_X \partial A(x)/\partial x$ consistent with the analysis of this simple case in Sec.3A.

Next, we describe the form of these diffusion fluxes for a linear lattice constituting a strict *single-file system* for different choices of D_{tr}. In the *hydrodynamic limit for large systems*, one has the exact result $D_{tr}(X) = 0$. This is a consequence of the anomalous nature of the diffusion of a tagged particle. Then, eq 5 gives the *exact hydrodynamic (h) diffusion fluxes*[22]

$$J_K(h) = -D_X[K(x)/X(x)]\partial X(x)/\partial x, \quad \text{for} \quad K = A \text{ or } B \quad (6)$$

This result follows directly from eq 5 and is also intuitively clear. The J_K must sum to the total diffusion flux which satisfies $J_X = -D_X \partial X(x)/\partial x$ for this noninteracting lattice-gas, and the individual fluxes are in proportion to the local species concentrations.

The *mean-field* (MF) *treatment* for a single-file system sets $D_{tr}(X) = D_X [1 - X]$ which yields chemical diffusion fluxes with the form

$$J_A(MF) = -D_X[1 - B(x)]\partial A(x)/\partial x - D_X A(x)\partial B(x)/\partial x \quad (7)$$

and an analogous expression applies for $J_B(MF)$. This result has been obtained previously by making simple MF-approximations for the conductivity in Onsager's transport theory,[17,18,47] and also from coarse-graining of a MF approximation to the discrete hierarchical master equations.[20,22,48] This MF form eq 7 can produce artificially high diffusion fluxes relative to eq 6.

Finally, we introduce a *perturbed hydrodynamic* (ph) *treatment* for a single-file system which is intended to account for finite system size (i.e., finite pore length, L). We first note that the tracer diffusion for finite 1D systems of L sites with periodic boundary conditions satisfies $D_{tr} = D_{tr}(X, L) = X^{-1}[1 - X]D_X/(L - 1)$ where the concentration is restricted to $X = m/L$ for m particles in the system.[49] For finite open systems of L sites where transport is *not* limited by adsorption−desorption at the pore ends, we use the effective form

$$D_{tr}(X, L) \approx [1 - X]D_X/[1 + X(L - 1)] \quad (8)$$

This choice is motivated by analogous expressions for D_{tr} applied in the analysis of membrane transport,[50] and by noting that eq 8 recovers the desired results that $D_{tr} \to 0$ as $X \to 1$, and $D_{tr} \to D_X$ as $X \to 0$. The requirement that transport is not adsorption−desorption limited in our modeling will be met by restricting consideration to cases where $W_{ads} + W_{des} \geq W_{diff}$. In our perturbed hydrodynamic treatment, we incorporate the expression 8 into the general form eq 5 for $J_K = J_K(ph)$.

The steady-state of our model has a constant particle concentration, $X(x) = X_{eq} = W_{ads}/(W_{ads} + W_{des})$. Thus, for the case of a *single-file system* treated above, the *steady-state diffusion fluxes* have the form

$$J_K(h) \to 0, \quad J_K(MF) \to -D_X(1 - X_{eq})\partial K(x)/\partial x, \quad \text{and} \quad J_K(ph) \to -D_{tr}(X_{eq})\partial K(x)/\partial x \quad (9)$$

as $X(x) \to X_{eq}$ (constant). In the hydrodynamic treatment, this result implies that the pore is populated only by the product B if all sites are catalytic; the pore can have nontrivial frozen concentration distributions in regions with no catalytic sites. These artificial features are erased in the perturbed hydrodynamic treatment. One anticipates that the mean-field treatment results in artificially large diffusion fluxes in the steady-state.

As noted above, we will compare the predictions of discrete versions of various RDE with results of KMC simulation for both transient and steady-state behavior. To this end, one must implement a natural discrete version of the diffusion fluxes. For the MF approximation, this is automatically provided from the master equations, and for other cases we utilize choices described elsewhere.[22]

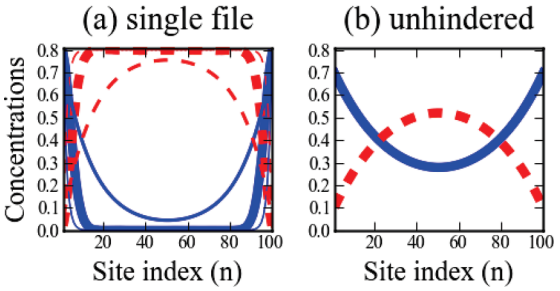

Figure 2. Steady-state concentration profiles for the A→B reaction for all sites catalytic: $W_{ads} = 0.8$, $W_{des} = 0.2$, $W_{diff} = 1$, $W_{rx}(A) = 0.001$, and $L = 100$. (a) Single-file diffusion: KMC, MF, and perturbed hydrodynamic results are shown as thick, moderate, and thin lines, respectively. (b) Unhindered passing (exact results). Solid blue lines $\langle A_n \rangle$; dashed red lines $\langle B_n \rangle$.

4. CONVERSION REACTIONS: KMC AND ANALYTIC RESULTS

4A. All Sites Catalytic (A→B). Here, we highlight the key features of steady-state behavior for our single-file A→B conversion reaction model, the shortcomings of popular mean-field treatments in describing this behavior, and the potentially far higher reactivity of systems with no single-file constraint. Our parameter choice is $W_{ads} = 0.8$, $W_{des} = 0.2$ (so $X_{eq} = 0.8$), $W_{diff} = 1$, with fairly low reaction rate $W_{rx} = W_{rx}(A) = 0.001$ which will amplify the above differences, for a pore of length $L = 100$. To analyze behavior, it is instructive to introduce the concept of a penetration depth, L_p, for reactant A. In the steady-state, one typically finds a roughly exponential decay of the concentration $\langle A_n \rangle \sim \exp(-n/L_p)$ into the pore for $n \ll L/2$, with possible deviations for the first few $n = 1,2,...$ sites.[20,22] Determination of L_p allows an assessment of steady-state reactivity since $R^B{}_{tot} \sim W_{rx}(A)\, L_p$. Figure 2a shows steady-state concentration profiles for single-file diffusion noting that $\langle X_n \rangle = \langle A_n \rangle + \langle B_n \rangle = X_{eq} = 0.8$ for all n. The small penetration for the exact KMC results (thickest line) with $L_p(KMC) \approx 2.6$ reflects single-file effects where the center of the pore is devoid of reactant and thus does not contribute to $R^B{}_{tot}$. The MF prediction, $L_p(MF) \approx 14.1$, greatly overestimates L_p because of artificial intermixing of A and

dx.doi.org/10.1021/cs200115c |ACS Catal. 2011, 1, 751–763

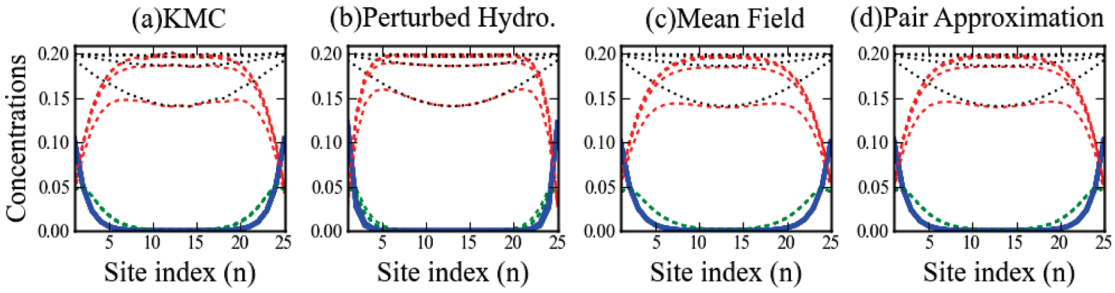

Figure 3. Concentration profiles for the A→B→C reaction for all sites catalytic: $W_{ads} = 0.2$, $W_{des} = 0.8$, $W_{diff} = 1$, $W_{rx}(A) = 0.4$, $W_{rx}(B) = 0.2$, and $L = 25$. Solid blue lines $\langle A_n \rangle$; short-dashed green $\langle B_n \rangle$; short-dashed red $\langle C_n \rangle$; dotted black $\langle X_n \rangle = \langle A_n \rangle + \langle B_n \rangle + \langle C_n \rangle$. (a) KMC simulation; (b) perturbed hydrodynamic treatment; (c) MF and (d) pair approximations. $t = 100$, 200, 300, and 400 where $\langle X_n \rangle$ and $\langle C_n \rangle$ increase with t.

B, and the pair approximation (not shown) does only slightly better with $L_p(\text{pair}) \approx 9.3$. The hydrodynamic treatment predicts essentially no penetration of the pore, and the perturbed hydrodynamic treatment does only slightly better with $L_p(\text{ph}) \approx 1.6$. None of these analytic treatments reliably captures behavior near the pore ends which is controlled by fluctuations in adsorption−desorption processes (a feature completely neglected in the standard hydrodynamic treatment).

To further understand the shortcomings of analytic theories, we note that the MF, pair, and also higher-order triplet approximations, and so forth,[51] naturally predict a functional dependence $L_p \sim (W_{rx}/W_{diff})^{-1/2}$ for $W_{rx}/W_{diff} \ll 1$. The perturbed hydrodynamic treatment actually predicts the same dependence, but with a much smaller prefactor. In contrast, simulation analysis (details not shown) indicates distinct non-MF behavior, $L_p \sim (W_{rx}/W_{diff})^{-n}$ for $W_{rx}/W_{diff} \ll 1$, where $n \approx 1/3$.[52]

Finally, we contrast single-file behavior with that for unhindered passing of A and B which can be determined analytically using the exact form of the fluxes $J_K^{n>n+1}$ described in Sec.2B. Figure 2b reveals a far greater penetration of reactant, A, into the pore in this case with $L_p \approx 31$. This feature and the associated higher reactivity are expected given the more facile diffusive transport.[24]

4B. All Sites Catalytic (A→B→C). In Figure 3, we show the time-evolution toward the *steady-state* for a pore of length $L = 25$, for the single-file A→B→C sequential conversion reaction where all sites are catalytic, $W_{ads} = 0.2$, and all species have the same hopping and desorption rates, $W_{des} = 0.8$, and $W_{diff} = 1$. We choose $W_{rx}(A) = 0.4$ and $W_{rx}(B) = 0.2$ low enough to ensure a significant population of A and B in the pore, but high enough so that center of pore is exclusively populated by C. Note that steady-state profiles for A and B are achieved quickly, but subsequent filling of the pore center (essentially just by C) occurs on a slower time scale. The steady-state has $\langle A_n \rangle + \langle B_n \rangle + \langle C_n \rangle = X_{eq} = 0.2$ for all n, but the hydrodynamic treatment would incorrectly predict that all interior sites are populated only by C with $\langle C_n \rangle = 0.2$. The perturbed hydrodynamic treatment is closer to the KMC results, but cannot correctly predict the extent of penetration of A and B into the pore. The mean-field and pair approximations capture the exact KMC behavior quite well in this case, but only because all rate parameters have similar magnitude.

Next, we consider transient behavior associated with *filling of a very long (semi-infinite) pore* for the single-file A→B→C reaction with all sites catalytic and the above parameters. Recall that the total concentration satisfies a standard discrete diffusion equation which reduces to the conventional continuum equation in the hydrodynamic regime. Thus, total concentration profiles collapse onto a single curve for increasing t after rescaling the n-axis by $(W_{diff}t)^{1/2}$. However, to achieve nontrivial scaling species profiles with significant populations of all species inside the pore, it is necessary to reduce the reaction rates as time is increased so that $W_{rx}(K) \cdot t$ remains constant for all K (see ref 22). More precisely, we find scaling solutions for the individual species concentrations of the form

$$\langle K_n(t) \rangle \approx X_{eq} F^K(n/(W_{diff}t)^{1/2}, W_{rx}(A)t, W_{rx}(B)t), \quad \text{for} \quad K = A, B, \text{ and } C \tag{10}$$

where $F^A(y,u,w) + F^B(y,u,w) + F^C(y,u,w) = F(y) = \text{erfc}(y/2)$. Here, erfc is the complementary error function and corresponds to the scaling solution for the classic nonreactive diffusion problem for a semi-infinite system.[53] Substitution of eq 12 into the hydrodynamic reaction-diffusion eqs 3a−3b consistently yields a closed coupled set of partial differential equations for the $F^K(y,u,w)$ (cf. ref 22).

The observations above on fluctuation effects suggest the following. (i) The MF and pair approximations should capture fluctuation-dominated behavior better for shorter t when most particles are close to the pore opening. (ii) The hydrodynamic treatment should better describe behavior for longer t where concentration profiles are smooth and broad. Indeed, this is the case as shown in Figure 4 where $W_{ads} = 0.2$, $W_{des} = 0.8$, $W_{diff} = 1$, and $W_{rx}(B) = 0.5W_{rx}(A)$ with fixed $W_{rx}(A) \cdot t = 4$. The peaks in $\langle B_n \rangle$ ($\langle C_n \rangle$) of around 0.05 (0.03) in the MF and pair approximations match KMC results for smaller t (larger W_{rx}), but these values persist for longer t. In contrast, the peak in $\langle B_n \rangle$ ($\langle C_n \rangle$) in the hydrodynamic treatment increases to about 0.09 (0.07) in good agreement with KMC results for longer t (smaller W_{rx}).

4C. Peripheral Sites Catalytic (A→B). We consider behavior for the A→B reaction for situations where contiguous strings of sites at each end of the pore are catalytic, but *not* those in the center. This type of distribution might result when catalytic sites are created by grafting after formation of a mesoporous material, in contrast to a co-condensation process.[3] An example of the results of KMC simulations for evolution to the steady-state is shown in Figure 5. The parameter choice is $W_{ads} = 0.8$, $W_{des} = 0.2$ (so $X_{eq} = 0.8$), $W_{diff} = 1$, and $W_{rx} = 0.001$, for a pore of length $L = 100$ (as in Sec.4A) with just 20 catalytic sites at each end.

Characterization of behavior is naturally divided into distinct regimes. First, in the *pore-filling regime*, some A successfully "runs the gauntlet" avoiding reaction in the peripheral catalytic regions and diffuses into the central noncatalytic region (Figure 5a). Second, after pore filling where $\langle X_n \rangle \sim X_{eq} \sim$ constant, a *metastable regime* persists for $\sim 10^3 - 10^4$ time units. In this regime, there is a peak in the quasi-static concentration of A (i.e., a "blob"

dx.doi.org/10.1021/cs200115c |ACS Catal. 2011, 1, 751–763

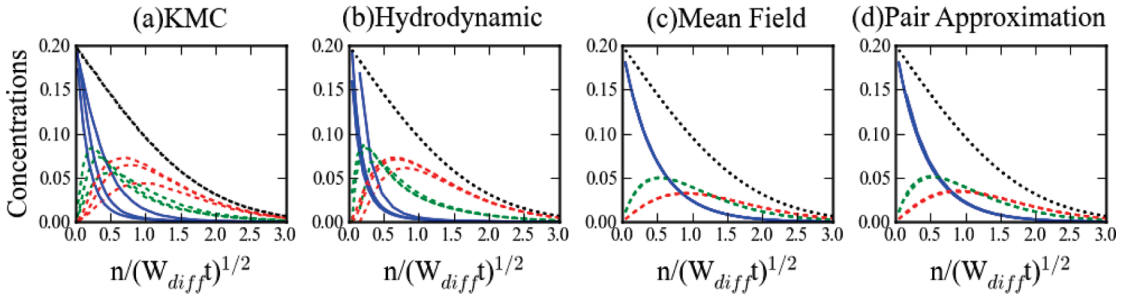

Figure 4. Scaled concentration profiles near the end of a semi-infinite pore for the A→B→C reaction with for all sites catalytic during pore filling: W_{ads} = 0.2, W_{des} = 0.8, W_{diff} = 1, $W_{rx}(B) = 0.5W_{rx}(A)$ with fixed $W_{rx}(A)\cdot t = 4$. (a) KMC for $W_{rx}(A)$ = 0.01, 0.0001, 0.000001. (b) hydrodynamic, (c) MF, and (d) pair approximations for $W_{rx}(A)$ = 0.1, 0.01, and 0.001. Solid blue lines $\langle A_n\rangle$; short-dashed green $\langle B_n\rangle$; short-dashed red $\langle C_n\rangle$; dotted black $\langle X_n\rangle$ (an erfc curve). B and C profiles increase (A decreases) with t.

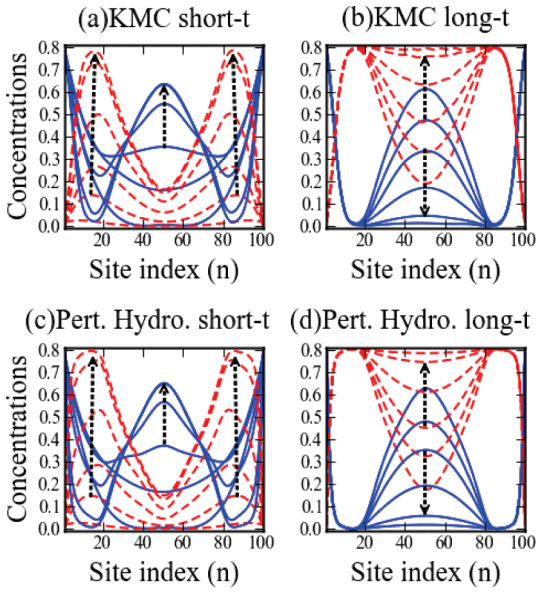

Figure 5. Complete evolution of species concentrations for the A→B reaction: W_{ads} = 0.8, W_{des} = 0.2, W_{diff} = 1, and W_{rx} = 0.001, and L = 100 with 20 catalytic sites at each end. Solid blue lines $\langle A_n\rangle$; dashed red $\langle B_n\rangle$. Top row: (a,b) KMC results. Bottom row: (c,d) perturbed hydrodynamic treatment. Left column: (a,c) pore-filling regime for t = 1, 5, 10, 20, 40, 60 ($\times 10^2$) where $\langle A_{50}\rangle$ grows. Right column: (b,d) late-stage evolution for t = 1, 5, 10, 20, 40, 60 ($\times 10^4$) where $\langle A_{50}\rangle$ decreases. Black dotted arrows: increasing t.

of A) in the center of the pore. Third and finally, there is a *slow relaxation regime*, where the population of A in the center of the pore decreases leading to the true steady-state where the pore center is almost devoid of A by $t \sim 10^6$ (Figure 5b). In fact, the final steady-state is very similar to that for a pore of length L = 100 with all sites reactive in Sec.4A (cf. Figure 2).

Figure 6 compares the KMC simulation results with predictions of analytic treatments for a finite time corresponding to the end of the pore-filling regime. The standard *hydrodynamic treatment* reasonably describes the concentration profile of the central A-blob in the KMC simulations, but evolves to a steady-state close to the profile shown. This "artificial" steady-state (which corresponds to the metastable state in the actual model), and a slight difference from KMC profile shape, derive from the neglect of fluctuations. In contrast, the *MF and pair approximations* (which incorporate artificially enhanced intermixing of A and B) fail completely to predict a significant peak in the concentration of A in central region. The pair approximation prediction (incorporating a somewhat better description of diffusion) is slightly closer to exact behavior. Significantly, the *perturbed hydrodynamic treatment* describes almost perfectly the shape of the A-profile in the noncatalytic pore center. Furthermore, this treatment eliminates the artificial steady-state of the standard hydrodynamic treatment and effectively describes evolution of concentration profiles in all three regimes (Figure 5c–d). The only shortcoming is in the description of concentration profiles near the pore ends (analogous to that noted in Sec.4A).

Finally, we describe in more detail the nature of fluctuation-dominated evolution in the last *slow relaxation regime*. The "blob" of A formed in the central noncatalytic region during pore filling is not frozen, but undergoes anomalous diffusion because of fluctuations allowing it to reach the peripheral catalytic regions. Eventually, essentially all of the A in this blob will be converted to B after a number of "collisions" with the catalytic regions. See Figure 7 for snapshots of this behavior from KMC simulations.

5. POLYMERIZATION REACTIONS: SYSTEMS AND MODELS

5A. $A + A_n \rightarrow A_{n+1}$ Polymerization Mechanism. Our modeling is motivated by studies of the formation of PPB within Cu^{2+}-functionalized MSNs.[34] In this example, A denotes the monomer, 1,4-diethynybenzene, for PPB formation and has a length of ~1 nm. In the experiments, the pore length was ~200 nm and diameter was ~2 nm. This catalyst material has a high loading of approximately 1 catalytic group per 2 nm^2 of pore surface.[34,54] MALDI mass spectroscopy measurements indicated that the average size of PPB oligomers corresponded to about 23 phenylene units (see ref 34, Supporting Information). ^{13}C solid-state NMR studies showed that these oligomers formed within and clogged the pores. Pore clogging is likely a general trend for polymerization in MSNs. Longer chains, composed of several hundred rings, were produced in MCM-41 materials during polymerization of aniline.[35] Another study reported an almost complete (up to 75%) filling of MCM-41 pore volumes with polymerized alkanes.[37]

Our modeling for the $A + A_n \rightarrow A_{n+1}$ polymerization mechanism assumes a single-file (no passing) constraint for monomers and polymers inside the pore. The pore is represented by a linear lattice with lattice constant corresponding to the monomer length and pore length L = 200. Monomers reside at lattice sites, and polymers form on contiguous strings of occupied sites. Certain

dx.doi.org/10.1021/cs200115c |ACS Catal. 2011, 1, 751–763

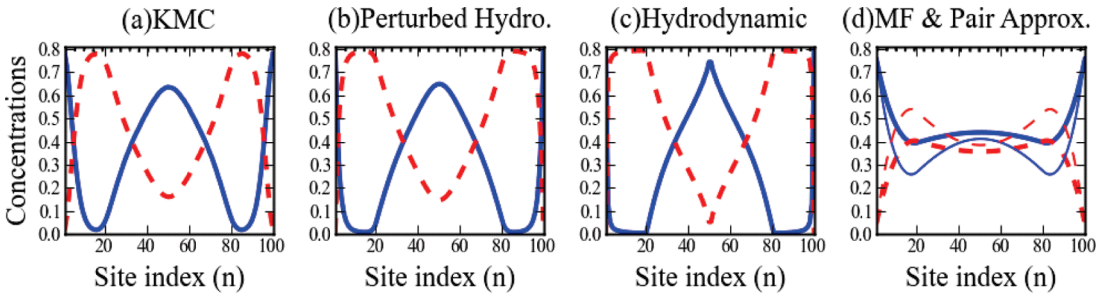

Figure 6. Behavior at the end of the pore-filling regime $t \approx 6000$ for the A→B reaction: $W_{ads} = 0.8$, $W_{des} = 0.2$, $W_{diff} = 1$, $W_{rx} = 0.001$, and $L = 100$ with 20 peripheral catalytic sites. Solid blue lines $\langle A_n \rangle$; dashed red lines $\langle B_n \rangle$. A in the pore center "ran the gauntlet" past catalytic regions. (a) KMC; (b) perturbed hydrodynamic; (c) hydrodynamic treatments; (d) MF (thicker lines), pair (thinner lines) approximations.

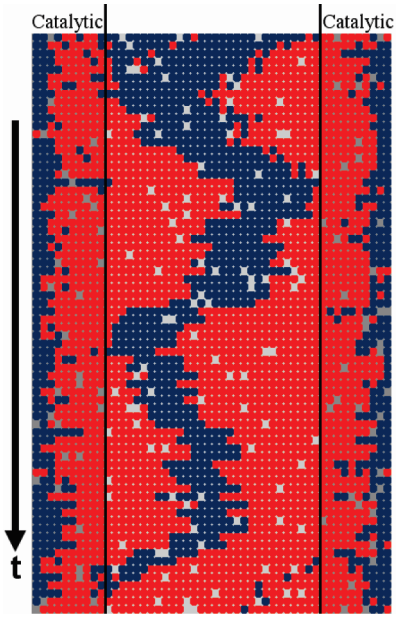

Figure 7. Sequence of KMC configurations ($\Delta t = 3000$) for late-stage evolution in a pore of length $L = 50$ with 10 catalytic sites (gray) on each end. Dark blue circles are A. Lighter red circles are B. Parameters: $W_{ads} = 0.9$, $W_{des} = 0.1$, $W_{diff} = 1$, and $W_{rx} = 0.0005$. Higher $X_{eq} = 0.9$ makes the A-blob more visible.

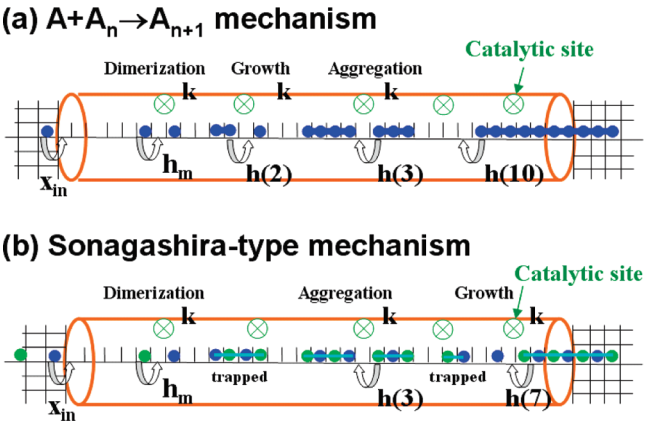

Figure 8. Schematics for (a) $A + A_n \rightarrow A_{n+1}$; and (b) Sonagashira-type polymerization mechanisms. Monomers A (B) are blue (green) circles. Processes illustrated include: dimerization [$A + A \rightarrow A_2$ for (a), and $A + B \rightarrow AB$ for (b)], growth [$A + A_{n>1} \rightarrow A_{n+1}$ for (a), and $A + BAB.. \rightarrow ABAB..$ for (b)], and aggregation [$A_4 + A_3 \rightarrow A_7$ for (a), and $BABA + BAB \rightarrow BABABAB$ for (b)].

sites within the pore are designated as catalytic, and dimerization ($A + A \rightarrow A_2$) as well as polymer growth ($A + A_{n>1} \rightarrow A_{n+1}$) and aggregation ($A_{n>1} + A_{m>1} \rightarrow A_{n+m}$) can occur only at these sites. The specific ingredients of the model (see Figure 8a) are as follows: (i) *Monomer adsorption* or input at rate x_{in} from the exterior of the pore to (unoccupied) end sites within the pore (ii) *Monomer hopping* to NN empty sites at rate h_m, including the possibility of hopping out of the pore. (iii) *Diffusion of polymers* of length l (measured in monomers or sites) by shifting the entire chain one site to the left or right with hop rate $h(l) = h_m/l^{\alpha}$ in each direction. (iv) *Partial and complete extrusion* of polymers via the same unbiased diffusion process as described above. However, once a linear polymer is completely extruded, it cannot return to the pore. (v) *Polymerization* at rate k at catalytic sites via processes described above where the end of the oligomer must be aligned with the catalytic site.

In our modeling, we will choose the monomer hop rate as $h_m = 1$ (which sets the time scale), the monomer input rate as $x_{in} = 0.1$, and the scaling exponent for the size-dependence of polymer diffusivity in the range $\alpha = 2-3$. The loading of catalytic sites can be characterized in terms of a mean separation, L_c, between such sites. Two special regimes are: (a) *Maximal catalyst loading* ($L_c = 1$) corresponding to the PPB experiments described above, and "small" reaction rate $k \leq 1$. In this work, we will consider this previously unexplored regime with $k \ll 1$, that is, reaction-limited kinetics. (b) *Low catalyst loading* ($L_c \geq 10$) and instantaneous reaction ($k = \infty$) at catalytic sites. This case of diffusion-limited reaction kinetics has been analyzed previously,[32,33,54] and is not discussed further here.

Dimerization $A + A \rightarrow A_2$ and growth $A + A_n \rightarrow A_{n+1}$ are particularly sensitive to the monomer density within the pore. Without reaction, the monomer concentration (per site) in the pore would increase to a uniform maximal value of $X_{eq} = x_{in}/(x_{in} + h_0)$ (≈ 0.1). Polymerization kinetics will clearly depend on the time to reach such densities relative to the characteristic time for reaction, $\tau_{react} \propto 1/k$. Thus, it is instructive to introduce a filling time, $\tau_{fill} = \tau_{fill}(p)$, for the concentration at the center of the pore to reach some fraction, p, of its maximal value in the absence of reaction. Then, it follows that

$$L \approx c_p [h_m \tau_{fill}(p)]^{1/2}, \quad \text{where} \quad c_{0.5} \approx 3.23, \quad c_{0.8} \approx 2.30, \quad \text{etc.} \tag{11}$$

dx.doi.org/10.1021/cs200115c |ACS Catal. 2011, 1, 751–763

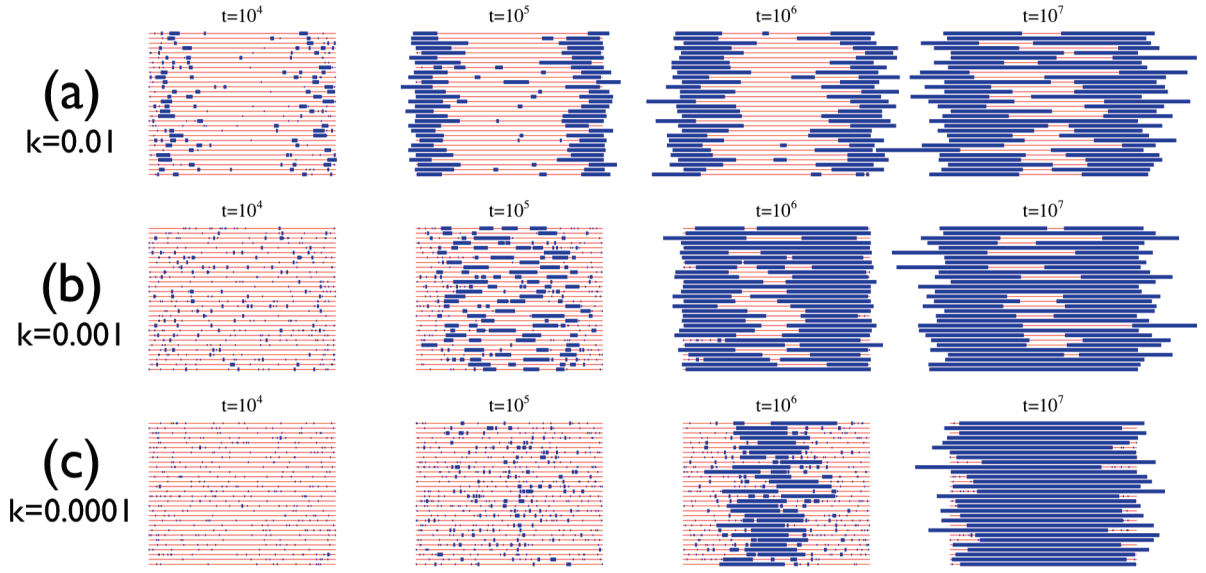

Figure 9. KMC simulation snapshots of A + $A_n \rightarrow A_{n+1}$ polymerization for $\alpha = 2$ and $L = 200$: (a) $k = 0.01$ (case II); (b) $k = 0.001$ (case III); (c) $k = 0.0001$ (case IV). Times $t = 10^4 - 10^7$ are shown. Polymers are in blue.

For our model ($L = 200$, $h_m = 1$), one has that $\tau_{fill}(0.5) = 3.8 \times 10^3$ and $\tau_{fill}(0.8) \approx 7.6 \times 10^3$.

5B. Sonagishira-Type Polymerization Mechanism. We will also briefly analyze the kinetics of a Sonogashira-type polymerization reaction. Our analysis is motivated by experiments[38,55] where a monomer A (1,4-diethylnylbenzene) and a monomer B (2,5-diakoxy 1,4-diiodobenzene) combine to form an AB-typed poly(phenylene ethynylene) (PPE) inside Pd(II)-functionalized mesoporous silica. Again, the pore length was ~200 nm and diameter was ~2 nm. Our modeling assumes a single-file (no passing) constraint for monomers and polymers inside the pore. Again monomers will reside on single sites of a linear lattice with lattice constant ~1 nm (the monomer length), and polymers will reside on contiguous strings of occupied sites. The pore length is $L = 200$ sites. Certain sites within the pore are designated as catalytic. Reaction of adjacent A-B units occurs at catalytic sites within the pore, but not of adjacent A-A or B-B units. This A-B reaction can involve two monomers (A + B→AB and B + A→BA), a monomer and a polymer (e.g., A + BABA..→ABABA..), or polymer−polymer aggregation (e.g., ..BAB+ABA..→..BABABA..).

The ingredients of the model are as for the simpler mechanism A + $A_n \rightarrow A_{n+1}$, except that there can be separate input rates and hop rates for A and B. However, in our modeling, we choose a common input rate $x_{in} = 0.1$, and hop rate $h_m = 1$ (which sets the time scale). The hop rate (in each direction) for polymers of length l again satisfies $h(l) = h_m/l^{\alpha}$ independent of the polymer termination, where we choose $\alpha = 2-3$. We consider only the case of maximal catalyst loading, $L_c = 1$, which is applicable in the experiments,[38] and "small" reaction rate $k \leq 1$. See Figure 8b for a schematic.

Contrasting the A + $A_n \rightarrow A_{n+1}$ mechanism where significant polymerization occurs, Sonagashira reactions could potentially evolve quite differently: the pore can be populated by many small oligomers and monomers which cannot react to undergo further polymerization when adjacent end units on neighboring oligomers are of the same type. Examples of such "trapped" species are shown in Figure 8b. Thus, one might expect inefficient polymerization for this Sonagashira mechanism in single-file systems.

6. POLYMERIZATION REACTIONS: GROWTH REGIMES AND KMC RESULTS

6A. A + $A_n \rightarrow A_{n+1}$ Polymerization Mechanism. The following results were obtained from our single-file diffusion model with monomer input rate $x_{in} = 0.1$, monomer hop rate $h_m = 1$, pore length $L = 200$, and maximal catalyst loading, $L_c = 1$. For our polymerization model, we can identify several reaction rate regimes based on distinct behavior during the initial stages of polymerization. These regimes, illustrated by KMC results in Figure 9, can be characterized as follows:

Case I: *large k*: initial rapid formation of a single larger polymer at each end of the pore.

Case II: *moderate k* (Figure 9a): initial formation of multiple polymers near the pore end during pore filling, that is, while there is a significant gradient in monomer concentration. Subsequent development of a dominant larger polymer near the pore opening occurs mainly by aggregation of smaller polymers. Note that the degree of polymerization in Figure 9a at time $t = 10^5$ corresponds roughly to the average length of PPB polymers relative to the pore size in our earlier experimental study.[34]

Case III: *low k* (Figure 9b): initial formation of multiple polymers throughout the pore after pore filling when the monomer density is fairly uniform. Subsequent development of a dominant larger polymer still near the pore opening occurs primarily by growth toward the opening (after an earlier aggregation stage).

Case IV: *very low k* (Figure 9c): initial formation of multiple polymers throughout the pore after pore filling. Subsequent formation of a single larger polymer near the pore center occurs by aggregation of smaller polymers.

The range of k values for these different cases depends on the exponent α for the size scaling of polymer diffusivity. Cases I through IV correspond to $k \geq 0.1$, $k \approx 0.01$, $k \approx 0.001$, and

dx.doi.org/10.1021/cs200115c |ACS Catal. 2011, 1, 751–763

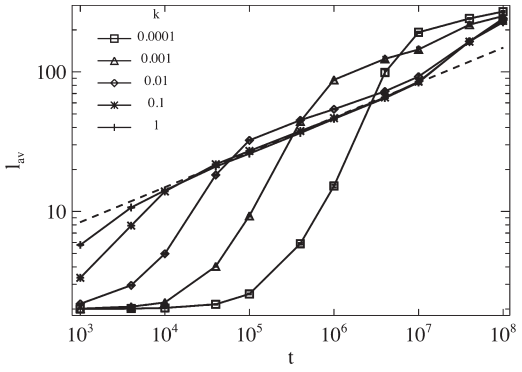

Figure 10. KMC simulation results for the average polymer length, l_{av} (measured in monomers) for $A + A_n \rightarrow A_{n+1}$ polymerization with $\alpha = 2$ and $L = 200$, for various values of reaction rate $k = 10^{-4}$ to 1 (shown). The dashed line has a slope $1/(\alpha + 2) = 1/4$ (reflecting temporal scaling for partial extrusion).

$k \leq 0.0001$, respectively, for $\alpha = 2$, and to $k \geq 0.1$, $k \approx 0.01$, $k \approx 0.001-0.0001$, and $k \leq 0.00001$, respectively, for $\alpha = 3$.

The above characterization describes only the initial behavior in each reaction rate regime. For Cases I−III, after the formation of a dominant larger polymer within the pore but near each end, there is a transition to a regime where this polymer is partly extruded from the pore opening. In this regime, the center of the pore between the two partly extruded polymers becomes denuded of monomers. In contrast for Case IV, partial extrusion of a single polymer out of both ends of the pore occurs when the polymer has grown to exceed the length of the pore. For either partial extrusion regime, further growth requires that an *extruded end of the polymer returns to just within the pore opening*. As a result, this regime of partial extrusion exhibits distinctive growth kinetics for the average polymer length, $l_{av} \sim (h_m t)^{1/(\alpha+2)}$, and non-Markovian growth kinetics for the polymer length distribution. See Sec.7 for details.

Now, we provide an analytic treatment of the initial polymer growth for **Cases II and III**, which is supported by KMC results in Figure 10. First, consider the onset of the formation of multiple polymers within some region of pore. After this onset at time $t \approx t_0$, further input of monomers to this region is effectively blocked by the polymer or oligomer closest to the pore end, so one has a local mass conservation tied to the monomer concentration $X = X_0 \leq X_{eq}$ at $t \approx t_0$. The values of t_0, X_0, and the location of this region will depend on the values of k and α. If $n_{av}(t)$ denotes the density per site of polymers (including monomers) within this region of the pore, then for reaction-limited polymerization kinetics,

$$dn_{av}/dt = -k(n_{av})^2 \quad \text{with} \quad n_{av} \approx X_0 \quad \text{at} \quad t \approx t_0 \qquad (12)$$

Thus, one has that

$$n_{av}(t) \sim X_0/[1 + X_0 k(t - t_0)] \quad \text{and}$$
$$l_{av}(t) \sim X_0/n_{av} \sim 1 + X_0 k(t - t_0), \quad \text{for} \quad t > t_0 \qquad (13)$$

Using eq 13 for $k \leq 0.001$ with $t_0 \sim \tau_{fill}(0.5) \sim 4 \times 10^3$ and $X_0 \sim 0.1$ effectively captures the basic features of initial polymer growth. For larger k, polymerization starts earlier so the effective t_0 and X_0 are smaller.

The above analysis only applies up until a time $t \approx t_1 \approx L/(2k) = 100/k$ where the polymer density drops to a value corresponding to about one polymer at each end of the pore. After this time, one has essentially one larger polymer at each end of the pore, and its growth is fed by an influx of monomers creating a local monomer density $X \sim X_{eq}$ at the end of the pore. This reaction-limited growth behavior is captured by $l_{av}(t) \approx X_{eq}k(t - t_1) + l_{av}(t_1)$ for $t_1 < t < t_{ex}$, where t_{ex} corresponds to the onset of partial extrusion. For $t > t_{ex}$, behavior crosses over to the partial extrusion regime described above where $l_{av}(t) \sim (h_m t)^{1/(\alpha+2)}$.

Finally, we briefly discuss the initial evolution in **Case IV**. Initial polymerization occurs uniformly throughout the pore after pore filling. However, the reaction rate is so low that there is a tendency for the smaller polymers formed closer to the ends of the pore to be extruded before they undergo significant growth and aggregation. This leaves a distribution of polymers closer to the pore center which aggregate into a single larger polymer. The growth kinetics in this initial stage is similar to Cases II−III, except that the increase in average polymer length is somewhat impeded by the loss of polymers from extrusion. However, once a single larger polymer has formed near the center of the pore at time $t = t_1$, say, it grows by aggregation of monomers with both ends, thus one might anticipate that $l_{av}(t) \approx 2X_{eq}k(t\text{-}t_1) + l_{av}(t_1)$. This regime will continue until $l_{av}(t) \approx L$ (the polymer length roughly matches the pore length). At that stage, one enters a regime of partial extrusion discussed further in Sec.7.

6B. Sonagishira-Type Polymerization Mechanism. As noted in Sec.5B, Sonagashira-type polymerization can be inhibited if the pore is populated by many small oligomers, where adjacent end units on neighboring oligomers are of the same type. However, the above analysis of the $A + A_n \rightarrow A_{n+1}$ mechanism suggests that such inhibition might be avoided by early formation of a dominant larger polymer near each end of the pore. Then, growth of this larger polymer either within the pore or after partial extrusion can occur by aggregation of monomers of alternating type which diffuse into the pore opening near the end of the polymer. The growth kinetics in this partial extrusion regime should be similar to that for the simpler $A + A_n \rightarrow A_{n+1}$ mechanism where the average polymer length increases like $l_{av}(t) \sim (h_m t)^{1/(\alpha+2)}$. However, for the Sonagashira mechanism, there will invariably be small oligomers trapped in the center of the pore between the two longer polymers. These trapped oligomers will block the aggregation of the two longer polymers, and may also ultimately inhibit their growth. Figure 11 illustrates the behavior described above for $\alpha = 2$ and also reveals the existence of distinct reaction rate regimes analogous to the $A + A_n \rightarrow A_{n+1}$ mechanism.

7. POLYMERIZATION REACTIONS: PARTIAL EXTRUSION REGIME

First, consider the $A + A_n \rightarrow A_{n+1}$ polymerization mechanism in the partial extrusion regime for a reaction rate corresponding to **Cases I−III**. In all these cases, a dominant larger polymer forms near each end of the pore which after reaching a length $l \sim l_0$ becomes partly extruded from one end of the pore. Then, further growth to lengths $l = l_0 + \Delta l$ requires that the extruded end of polymer returns to the interior of the pore. The extruded end of the polymer essentially undergoes a 1D random walk for which there are two possibilities. (i) With probability, $P_{ex}(l) \approx 1/l$ the polymer end travels a distance l from the end of the pore in which case the polymer is completely extruded,[33] so then the length of the polymer in the pore is reduced by $\delta l \approx -l$. (ii) With probability $P_{ret}(l) = 1 - P_{ex}(l)$, the polymer end returns to within the pore and typically grows by an amount $\langle \delta l \rangle = b > +1$.[33] Comparison (i) and (ii) indicates that overall polymer growth

dx.doi.org/10.1021/cs200115c |ACS Catal. 2011, 1, 751–763

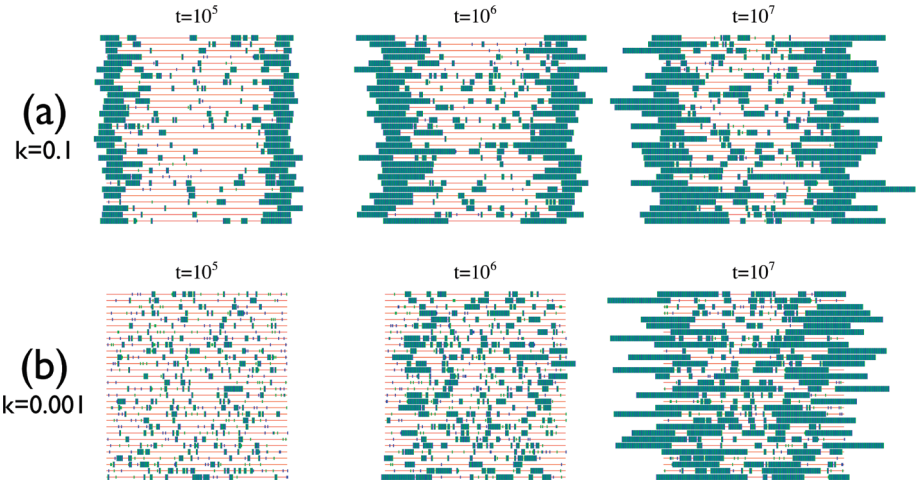

Figure 11. KMC simulation snapshots of polymerization for a Sonagashira-type mechanism for $\alpha = 2$ and $L = 200$. Examples are provided for (a) $k = 0.1$ (case II); and (b) $k = 0.001$ (case III). Times $t = 10^5 - 10^7$ are shown. A (B) type monomers are in blue (green).

dominates for polymers remaining in the pore. In fact, polymer growth can be captured by simplified modeling which neglects the possibility of complete extrusion.[33]

For a polymer of length l whose end has just left the pore opening, the typical number of hops, n, to return to the pore is given by $\langle n \rangle \approx l$.[33,56] Thus, as the polymer grows and $l \sim \Delta l \to \infty$, the mean number of hops to return diverges, and yet $P_{\rm ret}(l) \to 1$. This dichotomy between slow return and certain return as $l \to \infty$ derives from the unusual statistics of 1D random walks.[57] It reflects the existence of a long time-tail in the "return time distribution", $F_{\rm ret}(n) \sim (2\pi)^{-1/2}\, n^{-3/2}$, for larger n ($\ll l^2$).[33,57] The quantity $F_{\rm ret}(n)$ also encodes the statistics for multiple returns from which one can show that the mean number of returns in n hops satisfies $M(n) = (2n/\pi)^{1/2}$ for large n.[33,57] From this result, we can deduce the corresponding *polymer growth kinetics* since $\Delta l \approx M(n)b$. First, note that the number of hops taken by a growing polymer from the time of partial extrusion, $t_{\rm ex}$, to the current time, t, is roughly given by $n = \int_{t_{\rm ex}<t'<t} {\rm d}t'\, h(l = l_0 + \Delta l(t'))$. Thus, it follows that[33]

$$\Delta l(t) \approx M(n)b \approx (2/\pi)^{1/2} b \left[\int_{t_{\rm ex} < t' < t} {\rm d}t' h(l = l_0 + \Delta l(t')) \right]^{1/2} \quad (14)$$

Integrating the differential form of this identity yields the complete evolution of $\Delta l(t)$ for $t > t_{\rm ex}$,[58] in particular demonstrating the previously indicated asymptotic behavior

$$l_{av}(t) \sim \Delta l(t) \sim [\pi^{-1}(\alpha + 2) b^2 h_{\rm m} t]^{1/(\alpha+2)}, \quad \text{for} \quad \Delta l \gg l_0 \quad (15)$$

A simple Markovian rate equation approach, exploiting the feature that the rate of return of the end of the polymer to the pore scales like $l^{-1} h(l)$, can also recover eq 15.[32,33] However, this Markovian treatment completely fails to describe the behavior of the length distribution, N_l, of partially extruded polymers. This is a consequence of the presence of long time-tails in the return time distribution. However, the appropriate generalized Gamma distribution form

$$N_l \propto (l_{av})^{-1} (l/l_{av})^{\alpha/2} \exp[-b(\alpha)(l/l_{av})^{\alpha+2}] \quad (16)$$

together with eq 15 for l_{av} can be obtained from $F_{\rm ret}(n)$ using CTRW theory.[33]

Next, we consider the partial extrusion regime for the $A + A_n \to A_{n+1}$ polymerization mechanism for **case IV** of very low reaction rates. Now, the regime of partial extrusion corresponds to the polymer typically extending beyond both ends of the pore. This regime is initiated when the polymer length grows to be comparable to the pore length, that is, when $l \approx L$. Subsequent growth of a polymer of length $l = L + \Delta l$ requires that one of the two extruded ends of the polymer returns inside the pore (at which point growth occurs quickly given the low polymer mobility). Thus, the extruded ends of the polymer essentially undergo the same random walk over an interval of length Δl, and growth corresponds to this walk reaching either end of the interval. The first-passage time distribution for the number of hops before the walk reaches the end of the interval develops a long-time tail but only for large Δl. Thus, only for very large t would growth become sensitive to this long-time tail, producing simple asymptotic scaling like eq 15.

Finally, we briefly comment on polymer growth kinetics for the *Sonagashira-type mechanism* in the regime of partial extrusion from one end of the pore. As indicated in Sec.6B, the asymptotic scaling behavior of the average polymer length and even the form of the polymer length distribution, should be essentially the same as for the $A + A_n \to A_{n+1}$ mechanism discussed above. In both cases, polymer growth requires a return of the end of the polymer to within the pore, and it is the unusual statistics of the associated 1D random walk (i.e., a long time-tail in the return time distribution) which control behavior.

8. SUMMARY AND CONCLUSIONS

There have been several previous experimental and theoretical studies of *catalytic conversion reactions in single-file systems* primarily motivated by catalysis in zeolites. A picture has emerged for these systems of low reactivity localized near the pore openings, but a comprehensive and reliable theoretical framework is still lacking. Similarly, for conversion reactions in functionalized MSNs with narrow pores where passing of reactants and products can be severely constrained, there is also a need to provide a sound theoretical and modeling framework to enable appropriate interpretation and detailed analysis of experiments. This need

dx.doi.org/10.1021/cs200115c |ACS Catal. 2011, 1, 751–763

motivated the current contribution from which we can draw several key observations regarding behavior in these systems:

(i) *Dependence of reactivity on key rates*, specifically rates for reaction (W_{rx}) and diffusion (W_{diff}). The penetration depth, L_p, of reactant into the pore scales like $L_p \sim (W_{rx}/W_{diff})^{-n}$ for $W_{rx} \ll W_{diff}$, where $n \approx 1/3$. This is distinct from the prediction $n = 1/2$ of commonly accepted mean-field-type treatments. The scaling of L_p determines that of the overall reactivity since $R_{tot} \sim W_{rx}\, L_p$. As a consequence an Arrhenius analysis of reactivity, $R_{tot} \sim \exp[-E/(k_B T)]$, for temperature T yields the Arrhenius energy $E = (1 - n)E_{rx} + nE_{diff}$, where E_{rx} (E_{diff}) is the activation barrier for reaction (diffusion).

(ii) *Fluctuation-dominated reactivity*. The above scaling behavior of L_p reflects the feature that reactivity in single-file systems is controlled by fluctuations in adsorption−desorption processes near the pore openings. This underlies the failure of both traditional mean-field (or related higher-order pair, etc.) approximations, as well as the standard or perturbed hydrodynamic treatments introduced here.

(iii) *Pore diameter dependence on reactivity*. The overall reactivity increases dramatically upon relaxing the single-file constraint to allow some degree of passing of reactants and products (see Figure 2). This feature translates into a strong increase of reactivity with increasing pore diameter. We are currently analyzing such behavior for the conversion of PNB to an aldol compound in the presence of acetone in MSNs functionalized by catalytic amine groups. Experimental data is available for effective pore diameters ranging from 1.3 nm (very limited passing) to about 2.5 nm (facile passing) where these values account for both a reduction in diameter after functionalization by catalytic sites, and a further reduction during reaction by formation of a MSN-PNB adduct. A dramatic change from low to high yield is observed increasing pore diameter over this range.[31]

(iv) *Dependence on distribution of catalytic sites*. Functionalizing pores with catalytic sites just in the peripheral regions near the openings can result in concentration profiles quite distinct from the case with the entire pore being catalytic: some reactant can "run the gauntlet" past catalytic end regions to form a robust long-lived "blob" in the unreactive interior region (which eventually dissipates). However, in terms of reactivity, there is little difference from the case where all sites are catalytic, so functionalizing just near pore openings suffices to obtain optimal reactivity.

(v) *Predictive analytic formulations for spatiotemporal behavior*. Appropriate description of chemical diffusion is key in these systems. Yet, there has been lack of recognition of the existence of a hydrodynamic form eq 5 for diffusion fluxes which captures aspects of single-file diffusion, and a lack of utilization of this form. Use of eq 5 incorporating a simple form for tracer diffusion, D_{tr}, in finite systems captures almost perfectly the complex behavior described in (iv). For the fluctuation-dominated steady-state reactivity, preliminary analysis indicates the success of a treatment based on eq 5, with a heuristic form for D_{tr} varying from higher fluctuation-dominated values near the pore ends to lower single-file-controlled values in the pore interior.

We have considered here only the case of species-independent hop rates and desorption rates, in the absence of interactions between various species. Exploiting Onsager's transport theory and more general results for diffusion fluxes of the form of eq 5, one can show that basic features of chemical diffusion carry over to more general cases where species have unequal hop rates and interactions. Again, fluctuations control aspects of evolution and steady-state reactivity near pore openings, although some features of steady-state behavior differ from the case of species-independent rates.

For *catalytic polymerization reactions in single-file systems*, even a basic picture has been lacking for the spatiotemporal evolution of the monomer and oligomer distribution during polymerization. Our study has elucidated some universal features, including a partial extrusion regime with distinctive growth kinetics, which are common to different reaction mechanisms.

(i) *Formation of a long polymer near each pore opening*. For the simplest polymerization mechanism ($A + A_n \rightarrow A_{n+1}$) applicable to studies of PPB formation in Cu^{2+}-functionalized MSNs, there is a tendency for a broad range of reaction rates for a single dominant large polymer to be formed near each end of the pore.[32−34] These low-mobility sluggish polymers tend to clog the pore for long times, a feature observed in the experiments on PPB molecular wire formation,[34] and also in other systems.[35,37]

(ii) *Efficiency of the cross-coupling polymerization mechanisms* ($A + B \rightarrow AB$, $B+AB.. \rightarrow BAB..$, etc.). A natural expectation is that this mechanism will not be efficient for single-file systems because of the formation of many small oligomers within the pore which cannot react because of neighboring ends being of the same type. An experimental study of the Sonagashira reaction was performed in Pd(II)-functionalized MSNs which has a small effective pore diameter, because of the large size of the catalytic group.[38] Thus, this system mimics a simple single-file system given the large size of the PPE polymer, yet substantial polymerization was observed. We proposed that just as for the simpler $A + A_n \rightarrow A_{n+1}$ mechanism, a dominant larger polymer quickly forms near each end after which efficient growth is sustained by adsorption of monomers. This also leads to clogging. Our simulations and experiments support this picture.[55]

(iii) *Anomalous kinetics for the partial extrusion regime*. After formation of a long polymer within but near the pore openings, the system enters a partial extrusion regime. In this regime, further polymerization for single-file systems requires return of the extruded end of the polymer to within the pore. Thus, kinetics is sensitive to the unusual long time-tail in the associated return time distribution. On the basis of this observation, an appropriate non-Markovian CTRW treatment can be developed to describe both the unusual growth kinetics of the mean polymer length and even the polymer length distribution.

(iv) *Polymer length distributions*. The above CTRW analysis indicates that polymer length distributions for single-file systems are much broader than expected from a traditional Markovian rate equation prediction. Furthermore, they are expected to exhibit a generalized Gamma distribution scaling form. Current studies of the products of Cu-catalyzed oxidative polymerization of 1,6-dimethylphenol in fact reveal broad length distributions, but more detailed comparison with model predictions is required.[59]

In summary, utilization of the theoretical and modeling framework presented above for catalytic conversion and polymerization reactions in single-file systems allows us to address and elucidate numerous key issues listed above. When applied to specific catalytic reactions in nanoporous systems, this will enable more sophisticated analysis and interpretation of experimental data.

AUTHOR INFORMATION

Corresponding Author

*E-mail: evans@ameslab.gov.

Funding Sources

This work was supported by the Division of Chemical Sciences (Basic Energy Sciences), U.S. Department of Energy (USDOE) through the Ames Laboratory PCTC, Chemical Physics, and Catalysis projects. Ames Laboratory is operated for the USDOE by Iowa State University under Contract No. DE-AC02-07CH11358.

REFERENCES

(1) *Catalysis and adsorption by zeolites*; Ohlmann, G., Pfeifer, H., Fricke, G., Eds.; Elsevier, Amsterdam, The Netherlands, 1991.

(2) Beck, J. S.; Vartulli, J. C.; Roth, W. J.; Leonowicz, M. E.; Kresge, C. T.; Schmitt, K. D.; Chu, C. T. W.; Olson, D. H.; Sheppard, E. W. *J. Am. Chem. Soc.* **1992**, *114*, 10834–10843.

(3) Huh, S.; Wiench, J. W.; Woo, J.-C.; Pruski, M.; Lin, V.S.-Y. *Chem. Mater.* **2003**, *15*, 4247–4250.

(4) Tajima, K.; Aida, T. *Nanostructured Catalysts*; Plenum: New York, 2003.

(5) Reikert, L. In *Advances in catalysis*; Eley, D. D., Pines, H., Weisz, P. B., Eds.; Academic Press: New York, 1970; Vol.21, p 281.

(6) Kärger, J.; Freude, D. *Chem. Eng. Technol.* **2002**, *25*, 769–778.

(7) Harris, T. E. *J. Appl. Prob.* **1965**, *2*, 323–338.

(8) Fedders, P. A. *Phys. Rev. B* **1978**, *17*, 40–46.

(9) Nicolis, G., Prigogine, I. *Self-organization in Non-equilibrium Systems*; Wiley: New York, 1977.

(10) *Oscillations and Travelling Waves in Chemical Systems*; Field, R. J., Berger, M., Eds.; Wiley: New York, 1985.

(11) Ala-Nissila, T.; Ferrando, R.; Ying, S. C. *Adv. Phys.* **2002**, *51*, 949–1078.

(12) Imbihl, R.; Ertl, G. *Chem. Rev.* **1995**, *95*, 697–733.

(13) Engel, T.; Ertl, G. *Adv. Catal.* **1979**, *28*, 1–78.

(14) Evans, J. W.; Liu, D.-J.; Tammaro, M. *Chaos* **2002**, *12*, 131–143.

(15) Reuter, K.; Scheffler, M. *Phys. Rev. Lett.* **2003**, *90*, 046103.

(16) Liu, D.-J.; Evans, J. W. *Surf. Sci.* **2009**, *603*, 1706–1716.

(17) Krishna, R.; Vlugt, T. J. H.; Smit, B. *Chem. Eng. Sci.* **1999**, *54*, 1751–1757.

(18) Paschek, D.; Krishna, R. *Phys. Chem. Chem. Phys.* **2001**, *3*, 3185–3191.

(19) Tsikoyiannis, J. G.; Wei, J. E. *Chem. Eng. Sci.* **1991**, *46*, 233–253.

(20) Nedea, S. V.; Jansen, A. P. J.; Lukkien, J. J.; Hilbers, P. A. J. *Phys. Rev. E* **2002**, *65*, 066701.

(21) Nedea, S. V.; Jansen, A. P. J.; Lukkien, J. J.; Hilbers, P. A. J. *Phys. Rev. E* **2002**, *66*, 066705.

(22) Ackerman, D. M.; Wang, J.; Wendel, J. H.; Liu, D.-J.; Pruski, M.; Evans, J. W. *J. Chem. Phys.* **2011**, *134*, 114107.

(23) Okino, M. S.; Snurr, R. Q.; Kung, H. H.; Ochs, J. E.; Mavrovouniotis, M. L. *J. Chem. Phys.* **1999**, *111*, 2210–2221.

(24) Kärger, J.; Petzold, M.; Pfieffer, H.; S. Ernst, S.; Weitkamp, J. *J. Catal.* **1992**, *136*, 283–299.

(25) Rodenbeck, C.; Kärger, J.; Hahn, K. *J. Catal.* **1995**, *157*, 656–664.

(26) Rodenbeck, C.; Kärger, J.; Hahn, K. *Phys. Rev. E* **1997**, *55*, 5697–5712.

(27) Wang, X.; Chen, C.-C.; Chen, S.-Y.; Mou, Y.; Cheng, S. *Appl. Catal., A* **2005**, *281*, 47–54.

(28) Shouro, D.; Moriya, Y.; Nakajima, T.; Mishima, S. *Appl. Catal., A* **2000**, *198*, 275–282.

(29) Chen, H.-T.; Huh, S.; Wiench, J. W.; Pruski, M.; Lin, V.-S.-Y. *J. Am. Chem. Soc.* **2005**, *127*, 13305–13311.

(30) Chen, H.-T.; Trewyn, B. G.; Wiench, J. W.; Pruski, M.; Lin, V. S.-Y. *Top. Catal.* **2010**, *53*, 187–191.

(31) Slowing, I. I.; Ackerman, D. M.; Althaus; S. M. et al. 2011, in preparation.

(32) Liu, D.-J.; Chen, H.-T.; Lin, V.S.-Y.; Evans, J. W. *Phys. Rev. E* **2009**, *80*, 011801.

(33) Liu, D.-J.; Chen, H.-T.; Lin, V.S.-Y.; Evans, J. W. *J. Chem. Phys.* **2010**, *132*, 154102.

(34) Lin, V.S.-Y.; Radu, D. R.; Han, M.-K.; Deng, W.; Kuroki, S.; Shanks, B. H.; Pruski, M. *J. Am. Chem. Soc. (Commun.)* **2002**, *124*, 9040–9041.

(35) Wu, C.-G.; Bein, T. *Science* **1994**, *264*, 1757–1759.

(36) Llewellyn, P. L.; Ciesla, U.; Decher, H.; Stadler, R.; Schueth, F.; Unger, K. K. *Stud. Surf. Sci. Catal.* **1994**, *84*, 2013–2020.

(37) Cardin, D. J.; Constantine, S. P.; Gilbert, A.; Lay, A. K.; Alavaro, M.; Galletero, M. S.; Garcia, H.; Marques, F. *J. Am. Chem. Soc.* **2001**, *123*, 3141–3142.

(38) Chen, H.-T. Ph.D. Thesis, unpublished, Iowa State University, Ames, Iowa, 2003.

(39) Van Kampen, N. G. *Stochastic Processes in Physics and Chemistry*; North Holland: Amsterdam, The Netherlands, 1981.

(40) Kutner, R. *Phys. Lett.* **1981**, *81A*, 239–240.

(41) Evans, J. W. *Phys. Rev. B* **1990**, *41*, 2158–2162.

(42) Spohn, H. *Large Scale Dynamics in Interacting Particle Systems*; Springer: Berlin, Germany, 1991.

(43) Quastel, J. *Commun. Pure Appl. Math.* **1992**, *45*, 623–679.

(44) Tammaro, M.; Evans, J. W. *J. Chem. Phys.* **1998**, *108*, 7795–7806.

(45) Tammaro, M.; Evans, J. W. *Phys. Rev. E* **1998**, *57*, 5087–5094.

(46) Extension to the analogous multicomponent case is straightforward provided all species exchange with a common rate W_{ex}: the diffusion flux for A in the N-component case follows from the 2-component result lumping all the other $N - 1$ species into a single quasi-species.

(47) Zhdanov, V. P. *Surf. Sci.* **1988**, *195*, L217–221.

(48) Evans, J. W. *J. Chem. Phys.* **1992**, *97*, 572–577.

(49) van Beijeren, H.; Kehr, K. W.; Kutner, R. *Phys. Rev. B* **1983**, *28*, 5711–5723.

(50) Hodgkin, A. L.; Keynes, R. D. *J. Physiol. (London)* **1955**, *128*, 61–88.

(51) Evans, J. W. *Rev. Mod. Phys.* **1993**, *65*, 1281–1329.

(52) This estimate of $n \approx 1/3$ revises that in ref 22, and can be obtained from a modified hydrodynamic treatment incorporating a nonzero effective D_{tr} suitably decreasing away from the pore openings.

(53) Crank, J. *Mathematics of Diffusion*; Oxford University Press: Oxford, U.K., 1956.

(54) Modeling in ref 32 inappropriately assumed a low catalyst loading.

(55) Liu, D.-J.; Chen, H.-T.; Lin, V.S.-Y; Wiench, J. W.; Pruski, M.; Evans, J. W.; in preparation.

(56) Montroll, E. W.; Weiss, G. H. *J. Math. Phys.* **1965**, *6*, 167–181.

(57) Redner, S. *A guide to first-passage processes*; Cambridge University Press: Cambridge, U.K., 2001.

(58) One obtains $(\alpha+2)^{-1}[(1 + \Delta l(t)/l7^*)^{\alpha+2} - 1] - (\alpha+1)^{-1}[(1 + \Delta l(t)/l^*)^{\alpha+1} - 1] = \pi^{-1}b^2(l^*)^{-(\alpha+2)}\, h_m(t - t_{ex})$, with $l^* = l_0$ for case I-III, and $l^* = L$ for case IV.

(59) Hara, K.; Akahane, S.; Wiench, J. W.; Lin, V.S.-Y., Pruski, M.; Fukuoka, A.; in preparation.